Experimental study on the role of the target electron temperature as a key parameter linking recycling to plasma performance in JET-ILW

B. Lomanowski[1], M. Dunne[2], N. Vianello[3], S. Aleiferis[4], M. Brix[5], J. Canik[1], I.S. Carvalho[6], L. Frassinetti[7], D. Frigione[8], L. Garzotti[5], M. Groth[9], A. Meigs[5], S. Menmuir[5], M. Maslov[5], T. Pereira[6], C. Perez von Thun[10], M. Reinke[1], D. Refy[11], F. Rimini[5], G. Rubino[12], P.A. Schneider[2], G. Sergienko[13], A. Uccello[14], D. Van Eester[15], and JET Contributors[*]

[1] Oak Ridge National Laboratory, Oak Ridge, TN 37831-6169, USA
[2] Max Planck Institut für Plasmaphysik, Garching, Germany
[3] Consorzio RFX, Corso Stati Uniti 4, 35127 Padova, Italy
[4] NCSR 'Demokritos' 153 10, Agia Paraskevi Attikis, Greece
[5] CCFE, Culham Science Centre, Abingdon OX14 3DB, UK
[6] Instituto de Plasmas e Fusão Nuclear, Instituto Superior Técnico, Universidade de Lisboa, Portugal
[7] Fusion Plasma Physics, EES, KTH, SE-10044 Stockholm, Sweden
[8] Unità Tecnica Fusione, ENEA C. R. Frascati, via E. Fermi 45, 00044 Frascati (Roma), Italy
[9] Aalto University, PO Box 14100, FIN-00076 Aalto, Finland
[10] Institute of Plasma Physics and Laser Microfusion (IPPLM), Hery Str 23, 01-497 Warsaw, Poland
[11] Wigner Research Centre for Physics, POB 49, H-1525 Budapest, Hungary
[12] University of Tuscia, DEIM, Via del Paradiso 47, 01100 Viterbo, Italy
[13] Forschungszentrum Jülich GmbH, Institut für Energie- und Klimaforschung, Plasmaphysik, 52425 Jülich, Germany
[14] IFP-CNR, via R. Cozzi 53, 20125 Milano, Italy
[15] Laboratory for Plasma Physics Koninklijke Militaire School, Ecole Royale Militaire Renaissancelaan, 30 Avenue de la Renaissance B-1000, Brussels, Belgium

E-mail: lomanowskiba@ornl.gov

Abstract

Changes in global and edge plasma parameters ($H_{98(y,2)}$, dimensioneless collisionality ν^*, core density peaking, separatrix density $n_{e,sep}$) with variations in the D_2 fueling rate and divertor configuration are unified into a single trend when mapped to $\langle T_{e,ot}\rangle$, the spatially averaged spectroscopically derived outer target electron temperature. Dedicated JET with the ITER-like wall (JET-ILW) experiments in combination with an extended JET-ILW database of unseeded low-triangularity H-mode plasmas spanning a wide range of D_2 fueling rates, I_p, B_t and heating power have demonstrated the importance of $\langle T_{e,ot}\rangle$ as a key parameter linking the recycling particle source and detachment with plasma performance. The remarkably robust $H_{98(y,2)}$ trend with $\langle T_{e,ot}\rangle$ is connected to a strong inverse correlation between $\langle T_{e,ot}\rangle$, $n_{e,sep}$ and ν^*, thus directly linking changes in the divertor recycling moderated by $\langle T_{e,ot}\rangle$ with the established relationship between ν^*, core density peaking and pressure resulting in a degradation in core plasma performance with decreasing $\langle T_{e,ot}\rangle$ (increasing ν^*). A strong inverse correlation between the separatrix to pedestal density ratio, $n_{e,sep}/n_{e,ped}$, and $\langle T_{e,ot}\rangle$ is also established, with the rise in $n_{e,sep}/n_{e,ped}$ saturating at high $\langle T_{e,ot}\rangle$>10 eV in attached divertor conditions, consistent with the

*See the author list of 'Overview of JET results for optimising ITER operation' by J. Mailloux et al. to be published in Nuclear Fusion Special issue: Overview and Summary Papers from the 28th Fusion Energy Conference (Nice, France, 10-15 May 2021)"

observed $H_{98(y,2)}$ reduction as $\langle T_{e,ot} \rangle$ is driven from 30 to 10 eV via additional D_2 gas fueling. Consequently, the pronounced performance degradation in attached divertor conditions has implications for impurity seeding radiative divertor scenarios, in which $H_{98(y,2)}$ is already low (~0.7) before impurities are injected into the plasma due to moderate gas fueling requirements for promoting high divertor neutral pressure. A favorable pedestal pressure, $p_{e,ped}$, dependence on I_p has also been observed, with an overall increase in $p_{e,ped}$ at I_p=3.4 MA as $\langle T_{e,ot} \rangle$ is driven down from attached to high-recycling divertor conditions, in contrast to the lower I_p branches in which $p_{e,ped}$ is reduced with decreasing $\langle T_{e,ot} \rangle$. Further work is needed to clarify the potential role of edge opacity on the observed favorable pedestal pressure I_p scaling, as well as in projecting the global and edge plasma performance trends with $\langle T_{e,ot} \rangle$ to reactor-scale devices to improve predictive capability of the coupling between recycling and confined plasma fueling in what are foreseen to be more opaque edge plasma conditions.

1. Introduction

Understanding and controlling the properties of the recycled fuel species particle source, its poloidal distribution and penetration into the confined plasma region of a toroidal magnetic fusion device is important for achieving operational scenarios that can satisfy requirements for core plasma performance while ensuring the survivability of the surrounding vessel wall materials. In present day devices, recycled neutrals have been shown to significantly influence the structure and evolution of the density profile in the pedestal and scrape-off layer (SOL) regions of the edge plasma (e.g., [1] and references therein), with the midplane density at the separatrix recognized as an important interface parameter between the edge and core plasma (e.g., [2,3]). Decoupling the edge neutral source from excessive fueling of the confined plasma is a highly desirable attribute of core-edge compatible scenarios. While the degree of edge neutrals influence on the confined plasma is predicted to be reduced in large reactor-scale devices such as ITER due to improved neutral compression in the divertor and higher edge neutral opacity [1,4–6], experimental demonstrations linking divertor plasma parameters with pedestal and global performance parameters on current devices are needed to identify the governing physical processes constraining the compatibility of these plasma regions as well as for advancing the validation of SOL-edge-core integrated models.

In JET with the ITER-like wall (JET-ILW), increased gas puffing has been associated with reduced pedestal and global confinement [7–9]. Early on in ILW operations additional gas fueling requirements became necessary to suppress W sputtering and accumulation in the core plasma, which has led to an overall decrease in global confinement and pedestal pressure [7]. This degradation in performance compared to JET with Carbon wall (JET-C) has been at least partially recovered by operating in a divertor magnetic configuration in which the strike points are located close to the pump entrance (the corner-corner, CC, configuration) with increased pumping efficiency proportional to the neutral pressure at the pump entrance. As previously reported in [10,11], a strong influence of the divertor configuration on global confinement is correlated with large changes in the recycling patterns for the outer horizontal, outer vertical and corner-corner configurations. Using sub-divertor neutral pressure measurements, it was observed that the pumped particle flux increases as the outer strike point is moved towards the pump duct, with the highest performance obtained for the corner-corner configuration for a given fueling rate.

Recovery of the degraded plasma performance imposed by additional gas fueling in JET-ILW has been demonstrated in N_2 and Ne seeded H-mode integrated scenarios with the performance improvement attributed to suppression of ion temperature gradient (ITG) turbulence through core dilution leading to an increase in core T_i [12] and a recovery in $p_{e,ped}$ due to increasing $T_{i,ped}$ with sufficiently high heating power in high-δ Ne seeded scenarios [13], replicating similar benefits of N_2 seeding on $p_{e,ped}$ at lower input power [14]. A broad spectrum of core and pedestal transport and stability behavior is thus required to describe the integrated seeded scenario performance improvement.

The focus of the present work is to link the previous studies above with the electron temperature at the divertor target, $T_{e,t}$, which is the main parameter controlling divertor recycling and detachment. Whereas the main actuators are the auxiliary heating power, gas fueling rate and pumping efficiency – which depends on the divertor strike point location – the basic divertor physics parameter strongly correlating with the volumetric energy and momentum dissipation trends, thus leading to high recycling and detachment, is $T_{e,t}$ [15,16]. In the context of the JET-ILW gas fueling rate scans and divertor geometry impact on plasma confinement, correlations with $T_{e,t}$ have not been attempted thus far due to long-standing challenges associated with the

measurement and interpretation of the outer target electron temperature in the JET divertor in different magnetic configurations and over a range of plasma conditions.

The paper is organized as follows. Section 2 describes the dataset comprised of unseeded (pure deuterium) L-mode and H-mode fueling scans whereas in Section 3 the methodology for obtaining spectroscopic estimates of the outer target electron temperature is presented enabling the present study. These measurements provide, for the first time on JET-ILW, more accurate and routine estimates of the target electron temperature in the range 0.5-30 eV. In Section 4 correlations between the 'upstream' plasma parameters and the target electron temperature are presented, which unify previously disparate divertor configuration dependent trends mapped to the gas fueling rate. These new correlations are connected with previous dimensionless collisionality scans and the associated core and pedestal behaviors leading to performance degradation at high collisionality and low target electron temperature. In Section 4 the properties of the pedestal pressure in transitioning from low recycling to high recycling divertor conditions are also described, showing a favorable I_p scaling in pedestal pressure at high recycling conditions. The observations and their implications are summarized in Section 5.

A companion paper [17] expands on the results presented in this work with the aim of developing a consistent description of the relationship between divertor conditions and the midplane separatrix density, with emphasis on the applicability and limitations of reduced SOL models, such as the extended two-point model (2PM), in describing the main physical processes governing the scaling of the midplane separatrix density.

2. Dataset

Dedicated I_p=2 MA, B_t=2.3 T, low-δ unseeded H-mode discharges were carried out in different divertor configurations for the purpose of obtaining global and edge plasma parameter correlations with a consistent deuterium fueling and heating scheme. These discharges were heated with P_{NBI}=16 MW of neutral beam heating power and P_{ICRH}=2-3 MW of ion cyclotron resonance heating power, and fueled mainly by toroidally distributed gas introduction modules (GIMs) located at two poloidal locations on the high field (HFS) and low field (LFS) side in the divertor (Figure 1), with the total fueling rate, Γ_{D2}, varying in the range 0.8-10×10^{22} e^-/s. Figure 1 shows the different divertor configurations and the strike point proximity to the inner and outer pumping ducts, as well as the location of the cryopump. The configuration naming convention based on the position of the inner and outer strike points (ISP and OSP) are as follows: i) VH(C) and VH(D): inner vertical, outer horizontal tile 5 stack C and stack D; ii) VV: inner vertical, outer vertical; iii) CC: inner corner, outer corner; and iv) VC(T6): inner vertical, outer on top of tile 6, which is achieved by sweeping the OSP from the corner to the top of tile 6, with the ISP also being swept from the inner corner onto the inner vertical tile. A similar main chamber plasma shape was maintained as much as possible within the limitations of plasma shaping capabilities in configuring the divertor strike point positions (Figure 1). In particular, a ~10 cm upward vertical shift of the plasma could not be avoided in the VV configuration in order to place the inner and outer strike points on tiles 3 and 7, respectively.

To further test the sensitivity of the results to heating power, I_p and B_t, we compiled an expanded dataset of unseeded low-δ deuterium fueled discharges from the 2019-2020 JET-ILW experimental campaign with a range in beam heating power P_{NBI}=9-25 MW, P_{ICRH}=2-5 MW, I_p=1.5-3.4 MA, B_t=1.7-3.5 T and q_{95}=3-3.4. To obtain a large range in Γ_{D2} for the 3.4 MA, 3.5 T high performance, high power baseline scenario cases, we took advantage of a large increase in gas fueling that was introduced near the I_p ramp-down phase at the end of the discharge, with I_p varying at most 10% over the time window of interest.

To evaluate the quality of the outer target temperature measurements (Section 3), as well as to facilitate an assessment of the volumetric pressure-momentum and cooling loss trends described in the companion paper [17], we also carried out dedicated L-mode density ramp discharges in the four divertor configurations. Due to operational constraints and to avoid the L-H threshold in the VH configurations, the heating power variation in these discharges is in the range 1.1-2.5 MA.

3. Outer target electron temperature measurements

The primary diagnostic used for estimating the divertor electron temperature is the mirror-linked divertor spectroscopy system [18,19]. Figure 1 shows the vertical spectroscopy outer divertor lines of sight (LOS), with a spatial resolution of 17 mm. The divertor thermal electron temperature is inferred from the line-integrated Balmer photo-recombination continuum emission, as described in [20]. Inboard of the OSP the electron temperature estimates can be mapped to the region along the outer divertor leg and into the private-flux region (PFR) below the X-point, as inferred through synthetic spectroscopy post-processing of EDGE2D-EIRENE simulations [20,21]. These spatially resolved measurements are further complicated by the presence of reflections from the tungsten tile surfaces, and, although the influence of reflections on the radial T_e and n_e profiles has been estimated using the Cherab and Raysect codes [22,23], there remains uncertainty with respect to assumptions on the tungsten bidirectional reflectance distribution function, which likely vary spatially and temporally. Nevertheless, the synthetic spectroscopic results have shown that at the OSP, reflections have little impact below 10 eV. As a consequence of the highly

localized emission at the OSP, the spectroscopic $T_{e,OSP}$ estimates are within a factor of two of the 'actual' target values in the EDGE2D simulations, but, whereas in experiment $T_{e,OSP} \approx 0.5$ eV is regularly measured in conditions of pronounced detachment in L-mode density ramps, the synthetic spectroscopic results have so far not yielded $T_{e,OSP}$ below 1 eV in simulations with 'actual' values below 1 eV. Since the Bremsstrahlung emission in EDGE2D simulations depends on the spatial distribution of n_e and T_e, and is therefore influenced by the divertor plasma solution and the underlying assumptions on atomic physics processes and radial transport coefficients, reconciling the differences between synthetic measurement with experiment results is challenging in and of itself. Additionally, the 17mm spatial resolution combined with fluctuations in the position of the strike point over the 40 ms camera integration time result in moderate spatial smearing around the strike point, such that the electron temerature measurement near the OSP is more aptly described as a spatially averaged value around the OSP, $\langle T_{e,ot} \rangle$. The spectroscopic method yields measurements in the range $0.5 \leq \langle T_{e,ot} \rangle \leq 30$ eV, with larger uncertainty above 10 eV due to the reduced sensitivity in the Balmer photo-recombination edge height [20].

Allowing for the above limitations, Figure 2 shows the evolution of the spectrosopically and Langmuir probe (LP) derived radial T_e profiles from an L-mode density ramp with the OSP on the outer horizontal target in the VH(C) configuration. Early in the discharge the peaked spectroscopically inferred $T_{e,t}$ profile is in reasonable agreement with the LP $T_{e,t}$, indicating that the Bremsstrahlung emission is concentrated at the target. As the spectroscopic $T_{e,t}$ decreases, the radial profile starts to invert since the line-integrated signal away from the OSP corresponds to volumetric emission away from the target surface, while the emission near the OSP remains more localized. As the spectroscpoic $T_{e,t}$ decreases to 0.5 eV, the LP $T_{e,t}$ remains above 10 eV throughout the density ramp. It is reasonably to conclude from this comparison that the LP mesurements are not suitable for the present study due to known distortions of the probe current-voltage characteristics from kinetic effects leading to an overestimate of $T_{e,t}$ [24,25].

The VH(C) configuration is diagnostically optimized since the unobstructed view of the bulk tungsten tile 5 provides full spatially resolved spectroscopic radial profiles near the target. This level of detail is not available for diagnosing the outer target parameters in the VV and CC configurations due to the partially obstructed view and spectrometer viewing angle relative to the vertical target inclination (Figure 1). The outer target electron temperature spectroscopic measurement in the VV configuration is obtained from the chord closest to the OSP, and is considered an emission weighted average, $\langle T_{e,ot} \rangle$. In the case of the CC configuration, the OSP is often swept onto tile 6 as part of the thermal management of the surface temperature. Where the strike point is swept (with a typical frequency of 4 Hz) into the view of the divertor spectrometer on top of tile 6, direct measurement of $\langle T_{e,ot} \rangle$ is possible. In the case of a stationary OSP in the outer corner of tile 6 (as shown in Figure 1), a single LP provides ion saturation current, j_{sat}, measurements, but in this configuration the OSP is not in the view of the divertor spectroscopy system.

We have estimated an empirical correction factor in the CC configuration with the OSP out of view of the spectrometer by using the spectroscopic electron temperature estimate $\langle T_{e,ot} \rangle^{\text{outer-most}}$ from the outer-most unobstructed chord such that $\langle T_{e,ot} \rangle \approx 1.5 \langle T_{e,ot} \rangle^{\text{outer-most}}$ by noting the remarkable similarity in the peak-normalized integrated outer target ion current I_{ot} vs $\langle T_{e,ot} \rangle$ trends shown in Figure 3.a. This factor can be applied to the outer-most spectroscopy chord on the basis that the normalized I_{ot} vs $\langle T_{e,ot} \rangle$ trend in the CC configuration should overlap with the unified trend established for the other geometries. The physical justification for this assumption relies on the expectation that in the moderate to high-recycling regime with $\langle T_{e,ot} \rangle > 5$ eV above the I_{ot} saturation and rollover point in Figure 3.a, $I_{ot} \propto p_{e,u} T_{e,t}^{-1/2}$ with pressure conservation along the open field lines in the SOL from the upstream OMP to the divertor target [16] (i.e., $p_{e,u} \approx p_{e,t}$), with $T_{e,t}^{-1/2}$ being the main I_{ot} driver while the $p_{e,u}$ dependence is relatively weaker. For consistency throughtout this paper we consider attached divertor conditions at $\langle T_{e,ot} \rangle > 10$ eV, high recycling for $\langle T_{e,ot} \rangle < 10$ eV and pronounced (particle) detachment below roughly 2 eV corresponding to the I_{ot} rollover point. In [17] we discuss in detail the volumetric momentum and cooling loss measurements from the same L-mode density ramp discharges, with the pressure-momentum loss onset corresponding to the I_{ot} saturation point.

In the CC(T6) configuration with the OSP in view of the outer spectroscopy chord during the strike point sweeps, the $I_{ot} \propto p_{e,t} T_{e,t}^{-1/2} \propto n_{e,t} T_{e,t}^{1/2}$ trend (Figure 3.a, open symbols) is estimated using spectroscopically derived $n_{e,t}$ from D_δ Stark broadening measurements [26], since the inboard part of tile 6 lacks LP coverage. To confirm the validity of spectroscopic I_{ot} estimates, the I_{ot} vs $\langle T_{e,ot} \rangle$ trends were compared in the VH(C) configuration using both LP measurements and spectroscopy, with the two methods being in good agreement (not shown for clarity). The above procedure for estimating the $\langle T_{e,ot} \rangle$ correction in the CC configuration is only valid up to the I_{ot} rollover point, since additional data past the rollover point could not be obtained. While the empirically derived correction factor provides approximate $\langle T_{e,ot} \rangle$ estimates in the CC configuration, there is a clear need for direct measurements of the electron density and temperature at the outer corner tile 6 target to reduce uncertainty in the obtained values, as well as to provide spatially resolved target n_e and T_e profiles.

4. Target electron temperature correlations

With advances in the JET-ILW divertor density and temperature measurements described in Section 3 and in [20,21,26], it is now possible to compare the divertor configuration influence on the plasma performance on the basis of divertor physics parameters rather than the deuterium fueling rate, Γ_{D2}. As demonstrated from analysis of 2D plasma boundary simulation datasets [16,27], and supported by experiments [15,28,29], including from analysis of the JET L-mode discharges in the companion paper [17], the physical processes moderating divertor recycling behavior, neutral-plasma interactions and the associated volumetric power and momentum loss trends exhibit a primary dependence on the outer target electron temperature. Hence, the expectation is that $\langle T_{e,ot} \rangle$, the averaged outer target electron temperature measurement on JET-ILW, is a more suitable ordering parameter for comparing variations in recycling patterns in different divertor configurations, and should reconcile the impact of pumping efficiency with strike point position observed in [10,11].

The normalized I_{ot} rollover trends obtained from L-mode density ramps (Figure 3.a) serve as a valuable reference for the ELMy H-mode discharges for which the interpretation of inter-ELM recycling behavior is complicated by the ELM frequency and amplitude over the range of the Γ_{D2} (or $\langle T_{e,ot} \rangle$) scan. The divertor recycling response to ELMs is also compounded by the interplay of deuterium implantation and desorption dynamics on tungsten surfaces [30]. We have estimated I_{ot} for the subset of the H-mode dataset, namely the I_p=2MA, B_t=2.3 T, $P_{NBI} \approx$16 MW discharges, by ELM-filtering the LP j_{sat} data where possible, with the uncertainty in the I_{ot} estimates increasing with ELM-frequency and Γ_{D2}. The normalized I_{ot} trends for the VV, VH(C) and VH(D) configurations shown in Figure 3.b are consistent with the L-mode trends, albeit with a moderate I_{ot} underestimation for the VV and VH(D) configurations due to incomplete LP coverage at the OSP. The same normalization scaling factor was used to compare the three configurations, with the recycling at the outer target increasing monotonically with decreasing $\langle T_{e,ot} \rangle$. Data points with $\langle T_{e,ot} \rangle$ values below 1.5-2 eV, and hence in the prounced detached regime past the rollover point, could not be obtained at the moderate beam heating powers used as a result of operational limits due to beam reionization hot spots on the main chamber limiters with $\Gamma_{D2}>10^{23}$ e^-/s. Given the corespondence in the outer target recygling trends with $\langle T_{e,ot} \rangle$ between the L-mode and H-mode datasets, we have reasonably assumed that the empirical correction factor for $\langle T_{e,ot} \rangle$ estimates in the CC configuration obtained from the analysis of L-mode density ramps is equally valid in the H-mode discharges. The Balmer photo-recombination-based method for spectroscopically inferring the electron temperature, although limited to the 40 ms integration time, is intrinsically ELM-filtered since the emission is proportonal to $n_{e,t}^2$, with $n_{e,t}$ peaking during the inter-ELM phase. This has been confirmed by comparing ELM-averaged measurements with inter-ELM measurements during long (>40 ms) inter-ELM periods in the same steady-phase discharge.

4.1 Fueling rate and subdivertor pressure

The fueling rate as a function of $\langle T_{e,ot} \rangle$ is shown in Figure 4.a for the 2 MA dataset, including the VH(C), VH(D), VV and CC divertor configurations, and using a fueling scheme with 50-50% split in Γ_{D2} from toroidally distributed gas injection modules located near tile 8 and tile 4 in the poloidal cross-section (see Figure 1). The beam heating power in most of the 2 MA discharges was 15-16 MW (filled symbols in Figure 4.a), and in the remaining 2MA discharges at varying power levels in the range P_{NBI}=9-22 MW (open symbols in Figure 4.a). Moving the outer strike point towards the corner pump entrance (from VH(C) to VH(D) to CC), and hence increasing pumping efficiency, is shown to increase the required Γ_{D2} for a given value of $\langle T_{e,ot} \rangle$. On the other hand, an approximately equivalent $\langle T_{e,ot} \rangle$ response to Γ_{D2} is observed for VH(C) and VV, despite the differences in target inclination and relative position of the pump entrance (outer SOL in VH(C) vs. PFR in VV). For fixed Γ_{D2} and heating power, $\langle T_{e,ot} \rangle$ increases with the outer strike position shifting towards the pump entrance, hence modifying the divertor recycling regime towards lower recycling, consistent with the expectation of decreased influence of neutrals on the confined plasma. The datapoints corresponding to lower heating power levels (P_{NBI}=9-12 MW) for the VH(C) configuration at low $\langle T_{e,ot} \rangle$ are observed to deviate from the constant heating power trends, requiring somewhat lower fueling levels to reach the same value of $\langle T_{e,ot} \rangle$. The mixed power datapoints for the CC configuration are within the scatter of the fixed power cases. Hence, the ±40% change in heating power introduces roughly the same degree of variation in the Γ_{D2} vs $\langle T_{e,ot} \rangle$ trends.

The configuration dependence on the neutral molecular deuterium pressure in the subdivertor, p_{sub_div}, shown in Figure 4.b, is consistent with the Γ_{D2} trends, and hence the two are also considered to be well correlated, albeit with somewhat increased scatter in the VH(C) and VH(D) configurations due to the slow p_{sub_div} response time in combination with a shorter steady phase duration in some discharges. p_{sub_div} is measured by pressure gauges located about 2.5 m below the divertor pump entrance, and has been shown to be proportional to the neutral pressure at the pump entrance based on neutral gas flow simulations [31]. While the increased pumping efficiency in the CC configuration is clear in both the Γ_{D2} and p_{sub_div} trends, the pumping efficiency for the VV configuration appears to be somewhat higher than in the VH(C) and even VH(D) configurations as

indicated by the higher p_{sub_div}, especially in the lower $\langle T_{e,ot}\rangle$ cases, although the data scatter precludes a more meaningful analysis. This could be associated with variation in neutral pathways in the JET-ILW VV and VH configurations as a function of the target inclination [32] that lead to the observed differences in the Γ_{D2} and p_{sub_div} trends with respect to $\langle T_{e,ot}\rangle$, as well as differences with respect to the region of the plasma in the vicinity of the pump entrance: PFR in the VV configuration, with relatively higher neutral pressure compared to the outer SOL in the VH configurations.

The overall correlation between p_{sub_div} and Γ_{D2} is consistent with SOL parameter dependence studies on ASDEX-Upgrade (AUG) in which the neutral pressure is measured directly in the divertor, p_0 [33], but the p_{sub_div} slow response time on JET limits its usefulness in practice to discharges with long steady phases, relative to divertor physics parameters such as $\langle T_{e,ot}\rangle$, for which the response time is of the order of the ion sound speed in the SOL. More direct comparisons to the neutral pressure based $n_{e,sep}$ scaling obtained in AUG (see Section 4.3) would be possible with the addition of pressure gauges inside the JET vessel in similar locations, for example near the private flux region of the divertor plasma.

4.2 Plasma performance and collisionality

A strong correlation between the global confinement and collisionality has previously been observed in JET-ILW based on a dimensionless collisionality scan, $\nu^* \propto n_e Z_{eff}/T_e^2$, in low-δ plasmas achieved by means of changing the gas fueling rate [34]. The SOL density was also found to be correlated with the pedestal and volume averaged ν^*. The degradation of confinement with increasing collisionality was linked to changes in both the core plasma and pedestal. The reduction in the core plasma pressure was attributed to a decrease in the core density peaking in combination with a decrease in the core temperature via temperature profile stiffness, since even at constant pedestal pressure, the increase in $n_{e,ped}$ leads to a corresponding decrease in $T_{e,ped}$. The dependence of density peaking with collisionality has been observed on many devices [35–37], with recent studies on JET-ILW [38] predicting that about half of the density peaking originates due to neutral beam fueling and half due to an inward electron particle pinch. In the pedestal, increasing collisionality was found to degrade the pedestal stability, and thus the increase in $n_{e,ped}$ was balanced by a more pronounced decrease in $T_{e,ped}$, resulting in an overall reduction of the pedestal pressure, as was previously observed since re-establishing the type I ELM-y H-mode scenario in JET-ILW [14,39]. Figure 6 illustrates the decrease in core density peaking, temperature and total pressure profiles with decreasing $\langle T_{e,ot}\rangle$ (increasing Γ_{D2}) based on TRANSP [40,41] interpretive simulations of select 2 MA, 2.3 T discharges in the VH(C) configuration from the present dataset, with core T_e=T_i confirmed by main-ion charge exchange recombination spectroscopy [42].

Comparisons of the upstream and global plasma parameter trends with Γ_{D2} and $\langle T_{e,ot}\rangle$ are shown in Figure 5 for the entire low-δ data set described in Section 2. While the decrease in $H_{98(y,2)}$, global dimensionless collisionality (ν^*) and core density peaking ($n_{e,0}/\langle n_e\rangle$) are clearly correlated with increasing Γ_{D2}, the scatter in the trends attributed to the variation in the divertor configuration, and in particular the clear separation in the CC trends, is unified into a single trend when plotted against $\langle T_{e,ot}\rangle$. Thus, recasting the previously reported dimensionless collisionality trends in [34] in terms of $\langle T_{e,ot}\rangle$ links changes in the pedestal and core plasma directly to the divertor target conditions, intrinsically capturing the effect of varying pumping efficiency. Therefore, the strong $H_{98(y,2)}$ correlation with $\langle T_{e,ot}\rangle$ can be explained by a similarly strong correlation between $\langle T_{e,ot}\rangle$, $n_{e,0}/\langle n_e\rangle$ and ν^*, given the already established correlation between global confinement, ν^* and $n_{e,0}/\langle n_e\rangle$ [34,38]. However, a separation in the ν^* trends for the 1.5 MA branch which originates mainly from higher pedestal collisionality indicates that $\langle T_{e,ot}\rangle$ and ν^* are not simply interchangeable as independent parameters.

4.3 Outer mid-plane separatrix density

Since the core and pedestal collisionality are well correlated, and the SOL density is also correlated with the pedestal collisonality [34], the present focus is on elucidating the relationship between $\langle T_{e,ot}\rangle$, recycled neutrals and $n_{e,sep}$, the midplane separatrix density. $n_{e,sep}$ is an important interface parameter linking SOL and divertor physics to the pedestal, as most recently highlighted in a comparison of JET-C and JET-ILW gas scans in 2 MA, 2.3 T low-δ plasmas [43] in which a strong correlation between the pedestal pressure and the $n_{e,sep}/n_{e,ped}$ ratio was observed independent of the divertor configuration. Two distinct mechanisms were identified to explain the correlation depending on the value of $n_{e,sep}/n_{e,ped}$: i) an initial outward shift of the pedestal pressure and consequent reduction in the peeling-ballooning stability and pedestal height for $n_{e,sep}/n_{e,ped} < 0.4$; and ii) increased turbulent transport and possible resistive effects for higher $n_{e,sep}/n_{e,ped} > 0.4$. Given that pedestal models such as EPED [44] rely on values of the edge density as an input, improving our understanding of the dominant processes driving $n_{e,sep}$ and $n_{e,sep}/n_{e,ped}$ is critical for integrating the basic SOL and divertor physics with edge and core plasma performance, and in particular in existing machines in which fueling is thought to play an important role in driving the structure of the density pedestal (see [1] and references therein).

In the present H-mode dataset we observe a strong relationship between $n_{e,sep}$, $n_{e,sep}/n_{e,ped}$ and $\langle T_{e,ot}\rangle$, as shown in Figure 7.c. Whereas $n_{e,sep}$ was estimated assuming a constant $T_{e,sep}$=100 eV in [43], we have found that scatter in the $n_{e,sep}$ and $n_{e,sep}/n_{e,ped}$ trends with $\langle T_{e,ot}\rangle$ is reduced if the location of the separatrix is estimated by the often used two-point model (2PM) approximation for $T_{e,sep} \approx \left(7q_{\parallel,u}L/2\kappa_{0e}\right)^{2/7}$, in which $q_{\parallel,u}$ is assumed to be dominated by Spitzer parallel electron heat conduction [16], with $q_{\parallel,u} \approx \left(0.5P_{sep}/A\right)$ and $A \approx 2\pi R\lambda_q B_p/|B|$ (P_{sep}—power crossing the separatrix, λ_q—heat flux width estimated from the ITPA H-mode scaling [45], B_p—poloidal magnetic field, B—total magnetic field, R—major radius, κ_{0e}—electron parallel conductivity coefficient, L—connection length). The $n_{e,sep}/n_{e,ped}$ trend exhibits a steep rise as $\langle T_{e,ot}\rangle$ decreases and saturates at $\langle T_{e,ot}\rangle \approx 20$ eV with $n_{e,sep}/n_{e,ped} \approx 0.6$-0.8. Hence the outward pedestal pressure shift and accompanying reduction in $p_{e,ped}$ described in [43] with increasing $n_{e,sep}/n_{e,ped}$ corresponds to low recycling attached divertor conditions with relatively high $\langle T_{e,ot}\rangle$ > 20 eV, whereas at lower $\langle T_{e,ot}\rangle$ < 10 eV in the high recycling regime, the pedestal position is already saturated. Similar behavior is observed for the $H_{98(y,2)}$ trend with $\langle T_{e,ot}\rangle$, with a rapid $H_{98(y,2)}$ decrease as $\langle T_{e,ot}\rangle$ is reduced from 30 to 10 eV, and more gradual decrease at lower $\langle T_{e,ot}\rangle$ with $H_{98(y,2)} < 0.8$. Since the upper range of the spectroscopic $\langle T_{e,ot}\rangle$ measurement is limited to 30 eV, the cluster of points around $\langle T_{e,ot}\rangle$=30 eV in Figure 5 and Figure 7 likely includes cases at higher electron temperature which cannot be resolved. The steep trend at high $\langle T_{e,ot}\rangle$ probably extends to even higher values as the divertor regime nears sheath-limited conditions. In the companion SOL modelling paper [17], we attribute the rise in $n_{e,sep}$ during the steep $H_{98(y,2)}$ decrease at high $\langle T_{e,ot}\rangle$ – and consequently an increase in $n_{e,sep}/n_{e,ped}$ and ν^*, decrease in $n_{e,0}/\langle n_e\rangle$ and core pressure – to be driven mainly by the parallel pressure balance in the SOL due to increasing recycling and target pressure such that $n_{e,sep} \propto \langle T_{e,ot}\rangle^{-1/2}$, whereas volumetric cooling and momentum losses become the dominant $n_{e,sep}$ driving terms at $\langle T_{e,ot}\rangle$ < 10 eV in the $n_{e,sep}/n_{e,ped}$ saturation regime, with $H_{98(y,2)}$ already significantly degraded by that point. Hence, as is generally expected, but not hitherto quantified in these terms, in *unseeded* ELMy H-mode high-recycling JET-ILW scenarios in which target heat flux dissipation is achieved entirely by means of increasing the edge density via deuterium gas fueling (i.e., without extrinsic impurity seeding), divertor high recycling operation with $\langle T_{e,ot}\rangle$ < 10 eV is not compatible with high performance, low ν^* pedestal and core plasma conditions.

In Figure 7.a, the dependence of the separatrix density on changes in divertor configuration, I_p and B_t, combined with the overall increase according to $n_{e,sep} \propto \langle T_{e,ot}\rangle^{-1/2}$ via additional gas fueling, is also unified to a single trend by using the normalization $n_{e,sep} I_p^{-2/7} B_t^{-3/7}$, the origin of which is the basic 2PM scaling which yields $n_{e,sep} \propto q_{\parallel u}^{5/7} T_{e,t}^{-1/2} R q_{95}^{-2/7}$ (neglecting the volumetric loss terms) [2,16,46]. The robustness of this trend compared to the large scatter when plotted against Γ_{D2} in Figure 7.b demonstrates once again that $\langle T_{e,ot}\rangle$ is a more suitable ordering parameter for condensing the disparate $n_{e,sep}$ configuration dependent trends with Γ_{D2}, in particular for the CC configuration.

We have ignored the $P_{SOL}^{5/7}$ dependence in the $n_{e,sep}$ normalization as this results in a moderate separation of the 1.5 MA lower power points from the 2 MA and 3.4 MA branches. In fact, this almost linear power dependence, which originates from the assumption of dominant Spitzer parallel electron heat conduction relative to the convective contribution, (such that $T_{e,sep} \propto q_{\parallel u}^{2/7} R q_{95}^{2/7}$ is a weak function of input power), is at odds with the EUROfusion JET-ILW pedestal database scaling from [47], which yields $n_{e,sep} \propto I_p^{1.1} P_{in}^{-0.4} \Gamma_{D2}^{0.23}$ for constant values of triangularity. Although this scaling is based on a regression analysis with a relatively lower value of R^2=0.64 compared to the pedestal parameters, the negative power exponent clearly conflicts with the positive power scaling in the 2PM and demonstrates that further work is needed to understand, for instance, the importance of the convective vs conductive heat flux contributions and impact on the 2PM (e.g., [17,48,49]), in order to reconcile the two diverging power scalings. There is limited scope for elucidating the power dependence in the present study due to the relatively smaller dataset. Hence, replacing Γ_{D2} with $\langle T_{e,ot}\rangle$ in the regression of the EUROfusion JET-ILW pedestal database seems like a natural next step in order to incorporate the strong link between $\langle T_{e,ot}\rangle$ and $n_{e,sep}$.

A strong physics coupling between the separatrix density and the divertor neutral pressure, p_0, has been demonstrated on AUG such that $n_{e,sep} = 2.65\, p_0^{0.31}$ (10^{19} m^{-3}, Pa), where p_0, which can be considered an engineering parameter, is largely proportional to Γ_{D2} [33]. Direct comparison with the AUG scaling is not possible on JET due to a lack of in-vessel pressure gauges in the divertor, but it is reasonable to assume that, given the strong correlation between p_{sub_div} and Γ_{D2}, and p_0 and Γ_{D2} on AUG, a single point divertor pressure measurement correlated with $n_{e,sep}$ would not reconcile the configuration dependence in the Γ_{D2} vs $\langle T_{e,ot}\rangle$ trends shown in Figure 4. Ionization patterns, neutral pressure distributions and proximity to the pump entrance depend on the divertor configuration, as already noted in Section 4.1. Hence, as useful a scaling parameter as p_0 is in AUG and ITER studies with fixed vertical target divertor geometry [5,50,51], the more direct physics coupling between $\langle T_{e,ot}\rangle$ and upstream parameters should prove insightful when folded into a large dataset such as the EUROfusion pedestal database, which also spans the range of divertor configurations examined in the present work. In elucidating the recycling neutrals

influence on the edge pedestal and $n_{e,sep}$, development of a $\langle T_{e,ot} \rangle$ based scaling of edge plasma parameters is further motivated by the following observed target electron temperature dependencies: i) strong experimentally observed Lyman photon opacity correlation with $\langle T_{e,ot} \rangle$ independent of confinement regime and heating power in JET-ILW [20]; ii) strong correlation between $T_{e,t}$ and the molecular deuterium density in the divertor observed in edge plasma simulation datasets [52,53]; as well as iii) the primary dependence of volumetric momentum and cooling losses on $T_{e,t}$ observed in experiments and code datasets [16,17,28,29].

Estimates of the average atomic neutral density at the outer target, $\langle n_{D,ot} \rangle \Delta L$, inferred from absolutely calibrated spectroscopic measurements of D_α following the interpretation method in [20], also give a strong correlation with $\langle T_{e,ot} \rangle$, as shown in Figure 7.g and Figure 7.h. ΔL is the effective path length of D_α emission along the spectroscopic chord, which is generally difficult to estimate given that the emission distribution also changes with density and temperature, as demonstrated in [20]. While $\langle n_{D,ot} \rangle \Delta L$ estimates are considered reliable for the VH(C) and VH(D) configurations, a systematic underestimate is expected in the VV configuration since the outer-most chord does not directly intersect the OSP on tile 7. There is not enough information to yield reliable $\langle n_{D,ot} \rangle \Delta L$ estimates for the CC configuration given the obstructed spectroscopic view. Nevertheless, the obtained trends for the other configurations are consistent with the strong correlation between n_{D2} and $T_{e,t}$ observed from code datasets [16,52,53].

The link between the recycled neutral source, target electron temperature and separatrix density is assessed in more detail in the companion paper [17], in which 2D edge plasma modelling results indicate that while the divertor geometry has a significant impact on the neutral leakage from recycled neutrals in the divertor into the main chamber, the main chamber wall recycling also plays a strong role in driving $n_{e,sep}$, and is found to moderate the divertor geometry influence to the extent that only a large change in divertor geometry (e.g., removing the entire outer divertor baffle structure) can break the observed unification in $n_{e,sep}$ vs $\langle T_{e,ot} \rangle$ trends. In other words, the apparent lack of divertor geometry dependence in the $\langle T_{e,ot} \rangle$ trends with upstream parameters presented in this work can be explained rather simply by the relatively limited range of available divertor configurations in JET-ILW, coupled with the likely strong influence of main-chamber recycling. The caveat with this interpretation is that the assessment of the CC configuration with enhanced closure and high pumping efficiency is approximate, and can benefit greatly from direct spectroscopic access to the tile 6 divertor plasma from the measurement perspective, and from the modelling perspective by leveraging recent advances in SOLPS-ITER grid extension capabilities [54] for refining the fidelity of edge plasma simulations in the CC configuration.

4.4 Pedestal pressure

Figure 7.d shows $p_{e,ped}$ normalized by $p_{e,ped}$ at $\langle T_{e,ot} \rangle \approx 25$ eV as a function of $\langle T_{e,ot} \rangle$ and Γ_{D2} for the entire H-mode dataset. Whereas a reduction in $p_{e,ped}$ with increasing $n_{e,sep}/n_{e,ped}$ is shown in [43] for the 2 MA, 2.3 T discharges, the 2 MA, 2.3 T results mapped to $\langle T_{e,ot} \rangle$ in Figure 7.d reveal a non-monotonic trend with a steep $p_{e,ped}$ decrease at high $\langle T_{e,ot} \rangle$ consistent with the rise in $n_{e,sep}/n_{e,ped}$, followed by an inflection point at $\langle T_{e,ot} \rangle \approx 10$ eV in the saturated $n_{e,sep}/n_{e,ped}$ regime, although the scatter in the data increases considerably at lower $\langle T_{e,ot} \rangle$. Considering now the entire H-mode dataset, a favorable I_p dependence emerges, leading to an overall increase in $p_{e,ped}$ at 3.4 MA with decreasing $\langle T_{e,ot} \rangle$, in contrast to the lower I_p branches. This trend is more clearly illustrated in Figure 8, where $\langle T_{e,ot} \rangle$ is indicated by the color scale. For the same change in $\langle T_{e,ot} \rangle$ from 25 eV to ~few eV, $p_{e,ped}$ in the 3.4 MA branch is observed to increase by up to 50%, whereas a modest decrease in $p_{e,ped}$ is seen in the 2MA branch, and a more pronounced $p_{e,ped}$ decrease for the 1.5 MA branch. The $p_{e,ped}$ increase at 3.4 MA does not, however, lead to an increase in $H_{98(y,2)}$, implying that the collisionality and core density peaking scaling and the corresponding reduction of the core pressure with decreasing $\langle T_{e,ot} \rangle$ outweighs the relative changes in pedestal performance for the three I_p branches. It is not clear whether the favorable I_p scaling on $p_{e,ped}$ at low $\langle T_{e,ot} \rangle$ is linked to an increase in edge neutral opacity, since an increase in I_p increases the natural pedestal density, and hence reduces the ability of recycled neutrals to penetrate into the confined plasma with the penetration depth roughly $\propto 1/n_e$. On existing machines with relatively low edge opacity, neutral fueling of the confined plasma has been found to clearly influence the pedestal structure, but neutral fueling alone cannot fully explain changes in the pedestal structure, with transport predicted to play an increasingly dominant role in reactor-scale devices with opaque edge plasmas (e.g., [1] and references therein). Although the relative influence of neutral fueling vs transport on the density pedestal formation is outside the scope of this work, further studies focusing on an opacity scan on JET-ILW would be invaluable given that JET offers unique access to edge opacity regimes approaching ITER to within a factor of 2-3 at high I_p (3.5-4 MA) scenarios. Incorporating a wider I_p and Γ_{D2} range into previously attempted gas scan modulation experiments [55] for probing the electron density profile response is a promising route for clarifying the opacity effect, if a greater dynamic range can be obtained in the density profile response.

5. Summary

Replacing the gas fueling rate with the outer target electron temperature – the main physics parameter controlling divertor recycling and detachment – leads to a unification of several upstream parameter trends that otherwise depend on the divertor configuration. The previously reported [10,11] confined plasma performance increase attributed to improved pumping efficiency as a result of placing the strike point in closer proximity to the pump entrance has therefore been recast in terms of $\langle T_{e,ot} \rangle$, the spatially averaged outer target electron temperature, leading to a remarkably robust $H_{98(y,2)}$ trend in gas fueled, unseeded low-δ H-mode discharges spanning a large range in plasma current, neutral beam heating power, fueling rate, and four divertor configurations. The relationship between the target electron temperature and $H_{98(y,2)}$ is connected to a strong inverse correlation between $\langle T_{e,ot} \rangle$, $n_{e,sep}$ and ν*, where (i) increasing ν* is already known to be strongly correlated with a decrease in core pressure and confinement due to a decrease in core density peaking and pedestal and core temperature via stiff temperature profiles; and (ii) increasing $n_{e,sep}/n_{e,ped}$ is strongly linked with a decrease in pedestal pressure. As a result, the global and pedestal performance correlations with ν* and $n_{e,sep}/n_{e,ped}$, can now be linked directly with changes in the divertor recycling moderated by $\langle T_{e,ot} \rangle$. In unseeded scenarios, a steep H_{98} reduction and $n_{e,sep}/n_{e,ped}$ rise occur with $\langle T_{e,ot} \rangle$ decreasing from 30 to 10 eV, whereas, when the divertor reaches high recycling conditions with $\langle T_{e,ot} \rangle$<10 eV, the decay in $H_{98(y,2)}$ is more gradual and $n_{e,sep}/n_{e,ped}$ saturates. Hence, the bulk of the performance loss occurs before high recycling conditions are established in the divertor.

The observed correlation between Γ_{D2} and p_{sub_div} is consistent with a similar correlation on AUG between Γ_{D2} and p_0, the neutral pressure measured directly in the divertor. In the context of resolving the divertor configuration dependence in upstream parameter correlations, a single-point divertor neutral pressure measurement in JET-ILW will likely lead to a similar separation of the trends as with Γ_{D2}, in particular for the CC configuration, due to the divertor geometry influence on the neutral pressure distribution, ionization patterns and pumping efficiency. Hence, $\langle T_{e,ot} \rangle$ is not only a more suitable ordering parameter for reconciling the divertor configuration dependence in JET-ILW, but is also the main physics parameter amenable to validation of reduced SOL models like the extended 2PM. In normalizing $n_{e,sep}$ by plasma current and total magnetic field using the 2PM-based scaling $n_{e,sep} \propto I_p^{2/7} B_t^{3/7}$ to demonstrate the unification of the $n_{e,sep}$ trends with $\langle T_{e,ot} \rangle$, it also became apparent that the 2PM $P_{SOL}^{5/7}$ scaling conflicts with the $P_{loss}^{-0.4}$ scaling obtained from a regression on experimentally measured $n_{e,sep}$ from the EUROfusion pedestal database [47]. Further work is needed to extend the methodology presented in this work to the more comprehensive and wide-ranging EUROfusion pedestal database to resolve this discrepancy and improve understanding of the $n_{e,sep}$ dependence on global, edge and boundary physics parameters and dominant physics mechanisms.

While we have identified $\langle T_{e,ot} \rangle$ as an important ordering parameter linking edge plasma recycling with changes in the separatrix density and plasma collisionality, the detailed mechanisms concerning neutral leakage from divertor recycling, contributions to $n_{e,sep}$ from main chamber recycling, as well as the primary dependence of volumetric momentum and cooling losses on the target electron temperature, and the impact of these loss terms in moderating $n_{e,sep}$ are addressed in a companion paper [17] focusing on 2D edge plasma simulations and reduced 2PM interpretation.

The potential role of edge opacity on the observed favorable I_p scaling of the pedestal pressure as the divertor is driven to high-recycling and partially detached conditions needs to be clarified to improve understanding of the coupling between recycling and confined plasma fueling. While ITER edge plasma simulations suggest that a high divertor neutral compression can be decoupled from $n_{e,sep}$ and confined plasma fueling [5], it is not clear to what extent the observed strong correlation between $\langle T_{e,ot} \rangle$, $n_{e,sep}$, and $H_{98(y,2)}$ can be broken on existing devices, and to what extent the relationship between $\langle T_{e,ot} \rangle$ and $n_{e,sep}$ will hold in advanced divertors, and whether the predicted decoupling of the edge particle source from the core plasma will also extrapolate to compact, high field devices. The pronounced performance degradation in gas fueled plasmas in attached divertor conditions also has implications for impurity seeding radiative divertor scenarios with moderate levels of D_2 fueling, in which the reference unseeded plasmas are already characterized by low $H_{98(y,2)}$ ~0.7 before impurities are injected into the plasma, as, for example, in the vertical target Ne radiative fraction scan in JET-ILW [12]. Extending the JET unseeded H-mode dataset with impurity seeded scenarios will provide further insight into the relative role of gas fueled plasma performance degradation with decreasing $\langle T_{e,ot} \rangle$ (increasing Γ_{D2}) on the one hand, and on the other the influence of pedestal and core transport and stability changes on plasma performance recovery observed in high-power radiative scenarios with Ne seeding [12,13].

The approximate treatment of the corner configuration target temperature measurements in the present work warrants further studies of unseeded and impurity seeded scenarios in the corner configuration on JET-ILW, contingent on improved plasma temperature and density measurements with direct spectroscopic views of the outer corner divertor. This will facilitate the evaluation of integrated scenarios in the configuration with maximum closure and pumping efficiency, thus possibly offering core plasma performance improvements in detached divertor conditions.

Acknowledgements

This work has been carried out within the framework of the EUROfusion Consortium and has received funding from the Euratom research and training programme 2014–2018 and 2019–2020 under grant agreement No. 633053. The views and opinions expressed herein do not necessarily reflect those of the European Commission. This work was also supported by the US DOE under Contract No. DE-AC05- 00OR22725 with UT-Battelle, LLC.

References

[1] Mordijck S 2020 Overview of density pedestal structure: Role of fueling versus transport *Nucl. Fusion* **60**

[2] Leonard A W, McLean A G, Makowski M A and Stangeby P C 2017 Compatibility of separatrix density scaling for divertor detachment with H-mode pedestal operation in DIII-D *Nucl. Fusion* **57** 086033

[3] Kallenbach A, Bernert M, Dux R, Eich T, Henderson S S, Pütterich T, Reimold F, Rohde V and Sun H J 2019 Neutral pressure and separatrix density related models for seed impurity divertor radiation in ASDEX Upgrade *Nucl. Mater. Energy*

[4] Kukushkin A S, Pacher H D, Pacher G W, Kotov V, Pitts R A and Reiter D 2013 Consequences of a reduction of the upstream power SOL width in ITER *J. Nucl. Mater.* **438** S203–7

[5] Pitts R A, Bonnin X, Escourbiac F, Frerichs H, Gunn J P, Hirai T, Kukushkin A S, Kaveeva E, Miller M A, Moulton D, Rozhansky V, Senichenkov I, Sytova E, Schmitz O, Stangeby P C, De Temmerman G, Veselova I and Wiesen S 2019 Physics basis for the first ITER tungsten divertor *Nucl. Mater. Energy* **20** 100696

[6] Park J S, Bonnin X and Pitts R 2021 Assessment of ITER divertor performance during early operation phases *Nucl. Fusion* **61**

[7] Beurskens M N A, Schweinzer J, Angioni C, Burckhart A, Challis C D, Chapman I, Fischer R, Flanagan J, Frassinetti L, Giroud C, Hobirk J, Joffrin E, Kallenbach A, Kempenaars M, Leyland M, Lomas P, Maddison G, Maslov M, McDermott R, Neu R, Nunes I, Osborne T, Ryter F, Saarelma S, Schneider P A, Snyder P, Tardini G, Viezzer E and Wolfrum E 2013 The effect of a metal wall on confinement in JET and ASDEX Upgrade *Plasma Phys. Control. Fusion* **55** 124043

[8] Maggi C F, Saarelma S, Casson F J, Challis C, De La Luna E, Frassinetti L, Giroud C, Joffrin E, Simpson J, Beurskens M, Chapman I, Hobirk J, Leyland M, Lomas P, Lowry C, Nunes I, Rimini F, Sips A C C and Urano H 2015 Pedestal confinement and stability in JET-ILW ELMy H-modes *Nucl. Fusion* **55** 113031

[9] Frassinetti L, Saarelma S, Verdoolaege G, Groth M, Hillesheim J C, Bilkova P, Bohm P, Dunne M, Fridström R, Giovannozzi E, Imbeaux F, Labit B, De La Luna E, Maggi C, Owsiak M and Scannell R 2021 Pedestal structure, stability and scalings in JET-ILW: The EUROfusion JET-ILW pedestal database *Nucl. Fusion* **61**

[10] Tamain P, Joffrin E, Bufferand H, Järvinen A, Brezinsek S, Ciraolo G, Delabie E, Frassinetti L, Giroud C, Groth M, Lipschultz B, Lomas P, Marsen S, Menmuir S, Oberkofler M, Stamp M and Wiesen S 2015 Investigation of the influence of divertor recycling on global plasma confinement in JET ITER-like wall *J. Nucl. Mater.* **463** 450–4

[11] Joffrin E, Tamain P, Belonohy E, Bufferand H, Buratti P, Challis C D, Delabie E, Drewelow P, Dodt D, Frassinetti L, Garcia J, Giroud C, Groth M, Hobirk J, Jarvinen A E, Kim H T, Koechl F, Kruezi U, Lipschutz B, Lomas P J, De La Luna E, Loarer T, Maget P, Maggi C, Matthews G, Maviglia F, Meigs A, Nunes I, Pucella G, Rimini F, Saarelma S, Solano E, Sips A C C, Tsalas M, Voitsekhovitch I and Weisen H 2017 Impact of divertor geometry on H-mode confinement in the JET metallic wall *Nucl. Fusion* **57**

[12] Glöggler S, Wischmeier M, Fable E, Solano E R, Sertoli M, Bernert M, Calabrò G, Chernyshova M, Huber A, Kowalska-Strzęciwilk E, Lowry C, de la Luna E, Maggi C F, Stroth U, Sun H J, Reinke M L and Wiesen S 2019 Characterisation of highly radiating neon seeded plasmas in JET-ILW *Nucl. Fusion* **59** 126031

[13] Giroud C et al 2021 High performance ITER-baseline discharges in deuterium with nitrogen and neon-seeding in the JET-ILW *28th IAEA Fusion Energy Conferene (Virtual)*

[14] Giroud C, Maddison G P, Jachmich S, Rimini F, Beurskens M N A, Balboa I, Brezinsek S, Coelho R, Coenen J W, Frassinetti L, Joffrin E, Oberkofler M, Lehnen M, Liu Y, Marsen S, McCormick K, Meigs A, Neu R, Sieglin B, Van Rooij G, Arnoux G, Belo P, Brix M, Clever M, Coffey I, Devaux S, Douai D, Eich T, Flanagan J, Grünhagen S, Huber A, Kempenaars M, Kruezi U, Lawson K, Lomas P, Lowry C, Nunes I, Sirinnelli A, Sips A C C, Stamp M and Wiesen S 2013 Impact of nitrogen seeding on confinement and power load control of a high-triangularity JET ELMy H-mode plasma with a metal wall *Nucl. Fusion* **53**

[15] Loarte A, Monk R D, Martín-Solís J R, Campbell D J, Chankin A V, Clement S, Davies S J, Ehrenberg J, Erents S K, Guo H Y, Harbour P J, Horton L D, Ingesson L C, Jäckel H, Lingertat J, Lowry C G, Maggi C F, Matthews G F, McCormick K, O'Brien D P, Reichle R, Saibene G, Smith R J, Stamp M F, Stork D and Vlases G C 1998 Plasma detachment in JET Mark I divertor experiments *Nucl. Fusion* **38** 331

[16] Stangeby P C 2018 Basic physical processes and reduced models for plasma detachment *Plasma Phys. Control. Fusion* **60** 044022

[17] Lomanowski B *The role of the target electron temperature as a key parameter linking recycling to plasma performance II: separatrix density modelling*
[18] Meigs A, Stamp M, Igreja R, Sanders S and Heesterman P 2010 Enhancement of JET's mirror-link near-ultraviolet to near-infrared divertor spectroscopy system *Rev. Sci. Instrum.* **81**
[19] Lomanowski B A, Meigs A G, Conway N J, Zastrow K D, Sharples R M, Heesterman P and Kinna D 2014 Enhanced visible and near-infrared capabilities of the JET mirror-linked divertor spectroscopy system *Rev. Sci. Instrum.* **85** 0–5
[20] Lomanowski B, Groth M, Coffey I, Karhunen J, Maggi C F, Meigs A G, Menmuir S and O'Mullane M 2020 Interpretation of Lyman opacity measurements in JET with the ITER-like wall using a particle balance approach *Plasma Phys. Control. Fusion* **62** 065006
[21] Lomanowski B, Carr M, Field A, Groth M, Jarvinen A E, Lowry C, Meigs A G, Menmuir S, O'Mullane M, Reinke M L, Stavrou C K and Wiesen S 2019 Spectroscopic investigation of N and Ne seeded induced detachment in JET ITER-like wall L-modes combining experiment and EDGE2D modeling *Nucl. Mater. Energy* 100676
[22] Giroud D C, Meakins D A, Carr D M, Baciero D A and Bertrand M C 2018 CHERAB Spectroscopy Modelling Framework
[23] Carr M and Meakins A Raysect Python Raytracing Package (Version v0.4.0), (2017 December 11)
[24] Stangeby P C 1995 A problem in the interpretation of tokamak Langmuir probes when a fast electron component is present *Plasma Phys. Control. Fusion* **37** 1031–7
[25] Horacek J, Pitts R A, Stangeby P C, Batishchev O and Loarte A 2003 Predicted effects of parallel temperature gradients on the overestimation of TCV divertor target Langmuir probe Temeasurements *J. Nucl. Mater.* **313**–**316** 931–5
[26] Lomanowski B A, Meigs A G, Sharples R M, Stamp M and Guillemaut C 2015 Inferring divertor plasma properties from hydrogen Balmer and Paschen series spectroscopy in JET-ILW *Nucl. Fusion* **55** 123028
[27] Kotov V and Reiter D 2009 Two-point analysis of the numerical modelling of detached divertor plasmas *Plasma Phys. Control. Fusion* **51** 115002
[28] Lipschultz B, LaBombard B, Lisgo S and Terry J L 2007 Neutrals studies on alcator C-Mod *Fusion Sci. Technol.* **51** 390–400
[29] Paradela Pérez I, Scarabosio A, Groth M, Wischmeier M, Reimold F and Upgrade Team A 2017 SOL parallel momentum loss in ASDEX Upgrade and comparison with SOLPS *Nucl. Mater. Energy* **12** 181–6
[30] Brezinsek S, Wiesen S, Harting D, Guillemaut C, Webster A J, Heinola K, Meigs A G, Rack M, Gao Y, Sergienko G, Philipps V, Stamp M F, Jachmich S and Contributors J 2016 Characterisation of the deuterium recycling at the W divertor target plates in JET during steady-state plasma conditions and ELMs *Phys. Scr.* **T167** 014076
[31] Varoutis S, Gleason-González C, Moulton D, Kruezi U, Groth M, Day C, Wiesen S and Harting D 2017 Simulation of neutral gas flow in the JET sub-divertor *Fusion Eng. Des.* **121** 13–21
[32] Moulton D, Corrigan G, Harrison J R and Lipschultz B 2018 Neutral pathways and heat flux widths in vertical- and horizontal-target EDGE2D-EIRENE simulations of JET *Nucl. Fusion* **58** 096029
[33] Kallenbach A, Sun H J, Eich T, Carralero D, Hobirk J, Scarabosio A and Siccinio M 2018 Parameter dependences of the separatrix density in nitrogen seeded ASDEX Upgrade H-mode discharges *Plasma Phys. Control. Fusion* **60** 045006
[34] Frassinetti L, Beurskens M N A, Saarelma S, Boom J E, Delabie E, Flanagan J, Kempenaars M, Giroud C, Lomas P, Meneses L, Maggi C S, Menmuir S, Nunes I, Rimini F, Stefanikova E, Urano H and Verdoolaege G 2017 Global and pedestal confinement and pedestal structure in dimensionless collisionality scans of low-triangularity H-mode plasmas in JET-ILW *Nucl. Fusion* **57** 016012
[35] Angioni C, Peeters A G, Pereverzev G V., Ryter F and Tardini G 2003 Density Peaking, Anomalous Pinch, and Collisionality in Tokamak Plasmas *Phys. Rev. Lett.* **90** 4
[36] Weisen H, Zabolotsky A, Maslov M, Beurskens M, Giroud C and Mazon D 2006 Scaling of density peaking in JET H-modes and implications for ITER *Plasma Phys. Control. Fusion* **48**
[37] Greenwald M, Angioni C, Hughes J W, Terry J and Weisen H 2007 Density profile peaking in low collisionality H-modes: Comparison of Alcator C-Mod data to ASDEX Upgrade/JET scalings *Nucl. Fusion* **47**
[38] Tala T, Nordman H, Salmi A, Bourdelle C, Citrin J, Czarnecka A, Eriksson F, Fransson E, Giroud C, Hillesheim J, Maggi C, Mantica P, Mariani A, Maslov M, Meneses L, Menmuir S, Mordijck S, Naulin V, Oberparleiter M, Sips G, Tegnered D, Tsalas M and Weisen H 2019 Density peaking in JET-determined by fuelling or transport? *Nucl. Fusion* **59**
[39] Beurskens M N A, Frassinetti L, Challis C, Giroud C, Saarelma S, Alper B, Angioni C, Bilkova P, Bourdelle C, Brezinsek S, Buratti P, Calabro G, Eich T, Flanagan J, Giovannozzi E, Groth M, Hobirk J, Joffrin E, Leyland M J, Lomas P, De La Luna E, Kempenaars M, Maddison G, Maggi C, Mantica P, Maslov M, Matthews G, Mayoral M L, Neu R, Nunes I, Osborne T, Rimini F, Scannell R, Solano E R, Snyder P B, Voitsekhovitch I and Vries P De 2014 Global and pedestal confinement in JET with a Be/W metallic wall *Nucl. Fusion* **54**

[40] Breslau J, Gorelenkova M, Poli F, Sachdev J, Pankin A and Perumpilly G 2018 TRANSP
[41] Hawryluk R J 1981 AN EMPIRICAL APPROACH TO TOKAMAK TRANSPORT *Physics of Plasmas Close to Thermonuclear Conditions* ed B Coppi, G G Leotta, D Pfirsch, R Pozzoli and E Sindoni (Pergamon) pp 19–46
[42] Hawkes N C, Menmuir S, Giroud C, Meigs A, Conway N, Delabie E, Biewer T M and Hillis D L 2018 Instrumentation for the Upgrade to the JET Core Charge-Exchange 1–5
[43] Frassinetti L, Thun C P Von, Chapman B, Fil A, Hillesheim J C and Horvath L 2021 Role of the separatrix density in the pedestal performance in deuterium low triangularity JET-ILW plasmas and comparison with JET-C . *Accept. Publ. Nucl. Fusion*
[44] Snyder P B, Groebner R J, Hughes J W, Osborne T H, Beurskens M, Leonard A W, Wilson H R and Xu X Q 2011 A first-principles predictive model of the pedestal height and width: Development, testing and ITER optimization with the EPED model *Nucl. Fusion* **51**
[45] Eich T, Leonard A W, Pitts R A, Fundamenski W, Goldston R J, Gray T K, Herrmann A, Kirk A, Kallenbach A, Kardaun O, Kukushkin A S, LaBombard B, Maingi R, Makowski M A, Scarabosio A, Sieglin B, Terry J and Thornton A 2013 Scaling of the tokamak near the scrape-off layer H-mode power width and implications for ITER *Nucl. Fusion* **53** 093031
[46] Kallenbach A, Sun H J, Eich T, Carralero D, Hobirk J, Scarabosio A and Siccinio M 2018 Parameter dependences of the separatrix density in nitrogen seeded ASDEX Upgrade H-mode discharges *Plasma Phys. Control. Fusion*
[47] Frassinetti L, Saarelma S, Verdoolaege G, Groth M, Hillesheim J, Bilkova P, Boehm P, Dunne M G, Fridström R, Giovannozzi E, Imbeaux F, Labit B, de la Luna E, Maggi C F, Owsiak M and Scannell R 2020 Pedestal structure, stability and scalings in JET-ILW: the EUROfusion JET-ILW pedestal database *Nucl. Fusion*
[48] Leonard A W, Mahdavi M A, Allen S L, Brooks N H, Fenstermacher M E, Hill D N, Lasnier C J, Maingi R, Porter G D, Petrie T W, Watkins J G and West W P 1997 Distributed Divertor Radiation through Convection in DIII-D *Phys. Rev. Lett.* **78** 4769–72
[49] Casali L, Eldon D, Boedo J A, Leonard T and Covele B 2020 Neutral leakage, power dissipation and pedestal fueling in open vs closed divertors *Nucl. Fusion* **60**
[50] Kallenbach A, Bernert M, Dux R, Eich T, Henderson S S, Pütterich T, Reimold F, Rohde V and Sun H J 2019 Neutral pressure and separatrix density related models for seed impurity divertor radiation in ASDEX Upgrade *Nucl. Mater. Energy* **18** 166–74
[51] Kukushkin A S, Pacher H D, Pacher G W, Janeschitz G, Coster D, Loarte A and Reiter D 2003 Scaling laws for edge plasma parameters in ITER from two-dimensional edge modelling *Nucl. Fusion* **43** 716–23
[52] Sang C, Guo H Y, Stangeby P C, Lao L L and Taylor T S 2017 SOLPS analysis of neutral baffling for the design of a new diverter in DIII-D *Nucl. Fusion* **57**
[53] Stangeby P C and Sang C 2017 Strong correlation between D 2 density and electron temperature at the target of divertors found in SOLPS analysis *Nucl. Fusion* **57** 056007
[54] Dekeyser W, Boerner P, Voskoboynikov S, Rozhanksy V A, Senichenkov I, Kaveeva L, Veselova I, Vekshina E, Bonnin X, Pitts R A and Baelmans M 2021 Plasma edge simulations including realistic wall geometry with SOLPS-ITER *Nucl. Mater. Energy* **27** 100999
[55] Salmi A, Tala T, King D, Karhunen J, Mordijck S, Morales R B, Naulin V and Contributors J E T 2021 Gas scan to probe fuelling through the H-mode pedestal in JET *47th EPS Conference on Plasma Physics, EPS 2021* Europhysics Conference Abstracts (France: European Physical Society)

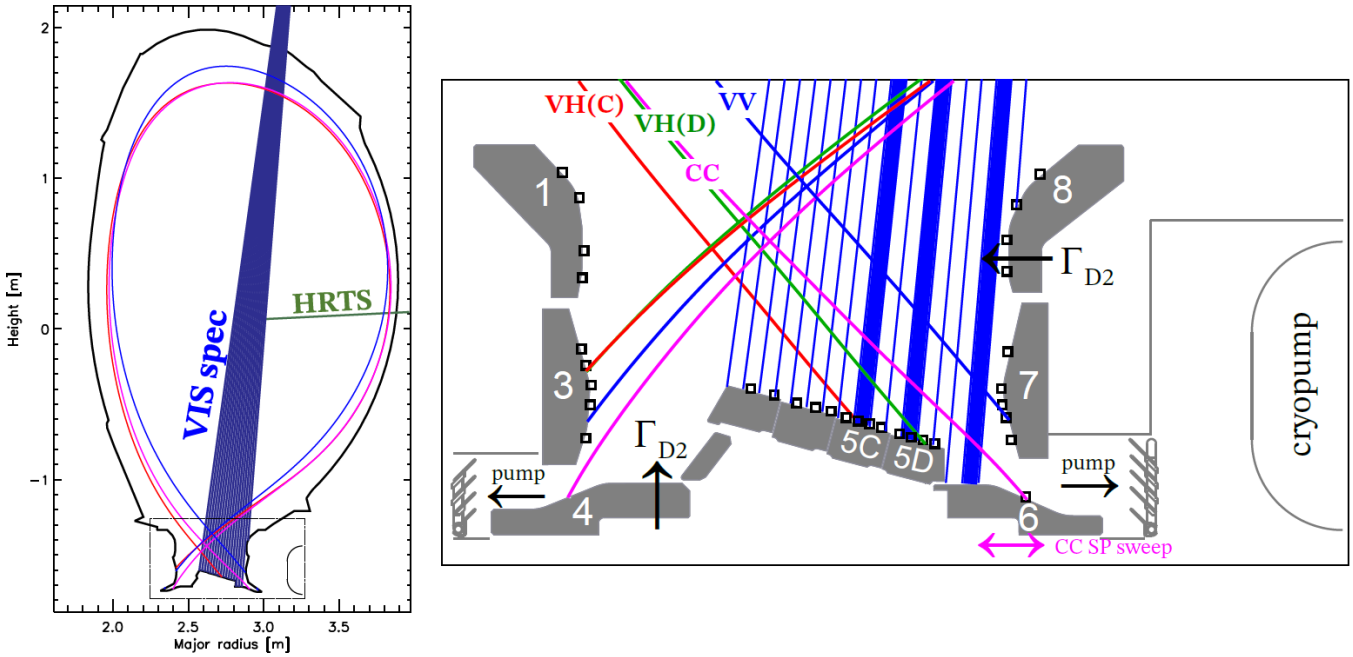

Figure 1: (left) JET-ILW diagnostic lines of sight including the visible divertor spectroscopy system and the high resolution Thomson scattering (HRTS) system. (right) Divertor configurations, including; i) inner vertical, outer horizontal with outer strike point on tile 5 stack C and D, VH(C) and VH(D), respectively; ii) vertical-vertical, VV, configuration; and iii) corner-corner, CC, configuration. The spectroscopy chords used to evaluate $\langle T_{e,ot} \rangle$ are shaded in, with the outer-most shaded chord used for both the VV and the CC configurations, in combination with the empirical correction factor (CC only). Also shown are the extent of the outer strike point sweep in the CC configurations, as well as the poloidal locations of the toroidally distributed gas introduction modules typically used to fuel the unseeded H-mode scenarios.

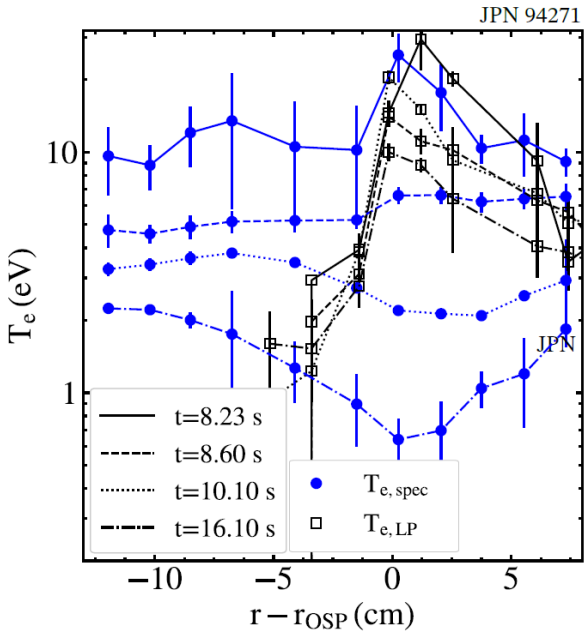

Figure 2: Comparison of outer target radial T_e profile measurements obtained from spectroscopy and LPs during an L-mode density ramp discharge in the VH(C) divertor configuration.

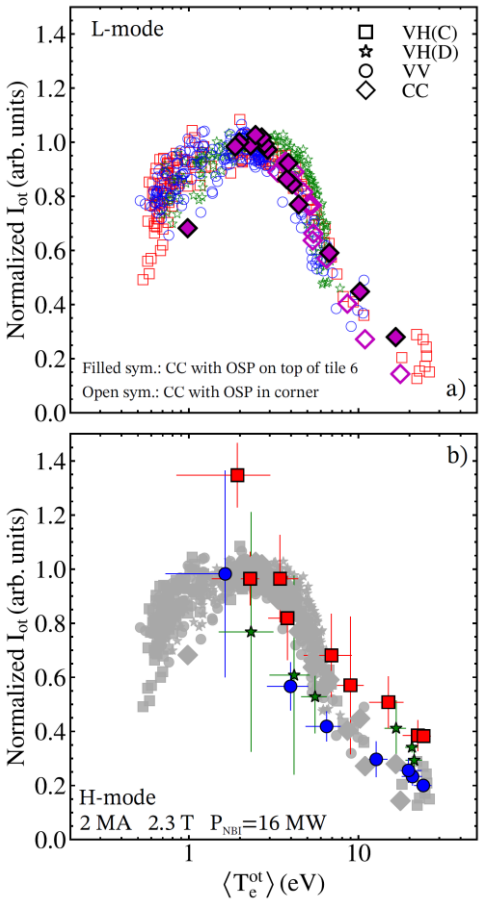

Figure 3: Normalized outer target ion current, I_{ot}, from L-mode density ramps (a) and H-mode 2MA, 2.3T gas scan dataset with 16 MW of beam heating, based on inter-ELM LP j_{sat} measurements (b). Open symbols in (a) refer to the CC configuration with the OSP located in the corner of tile 6 with the spectroscopy view obstructed by the outer divertor tiles 7 and 8, whereas filled symbols denote spectroscopically derived I_{ot} with the OSP located on top of tile 6 within the view of spectrometer chords.

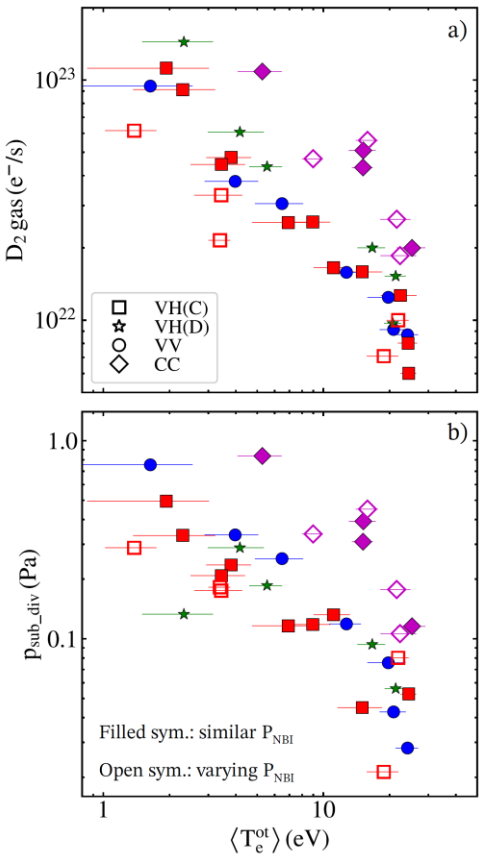

Figure 4: Correlations between $\langle T_{e,ot} \rangle$ and D_2 gas fueling rate (a) and sub-divertor neutral pressure (b) for the 2MA, 2.3T H-mode dataset. Filled symbols denote discharges with similar beam heating power (16 MW), whereas open symbols denote discharges with varying beam heating power in the range 9-22 MW.

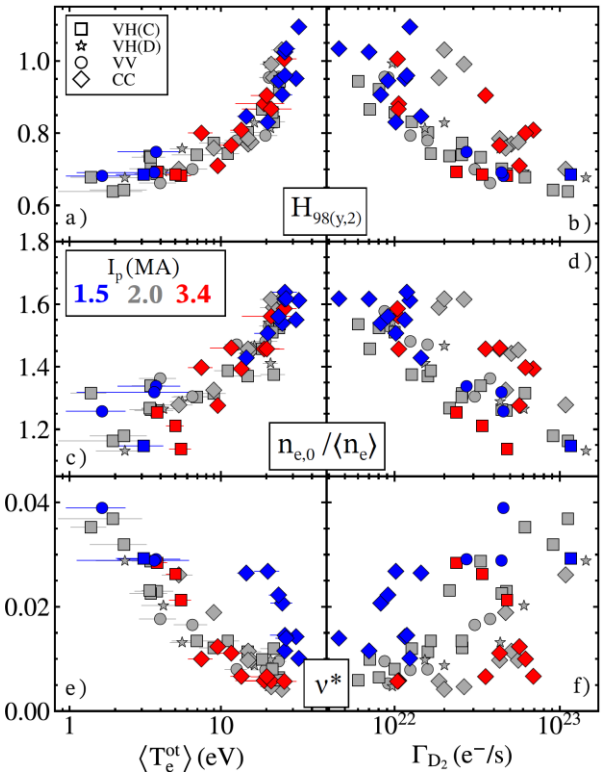

Figure 5: Correlations between $\langle T_{e,ot} \rangle$ (a,c,e) and D_2 gas fueling rate (b,d,f) and $H_{98(y,2)}$, core density peaking, $n_{e,0}/\langle n_e \rangle$, and global collisionality, ν*, spanning the entire H-mode unseeded dataset. The colors highlight the three different plasma current branches of the dataset.

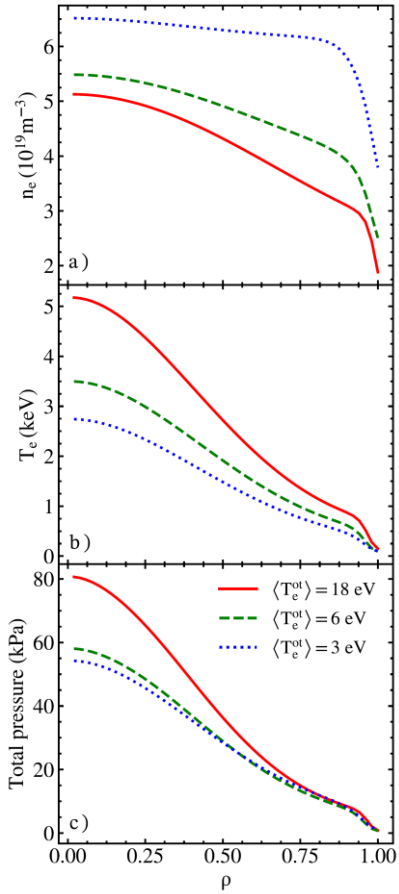

Figure 6: Electron density and temperature radial profiles and total pressure obtained from TRANSP interpretive simulations of select 2MA, 2.3T unseeded H-mode discharges with 16 MW of beam heating, mapped to ρ=ψtor1/2.

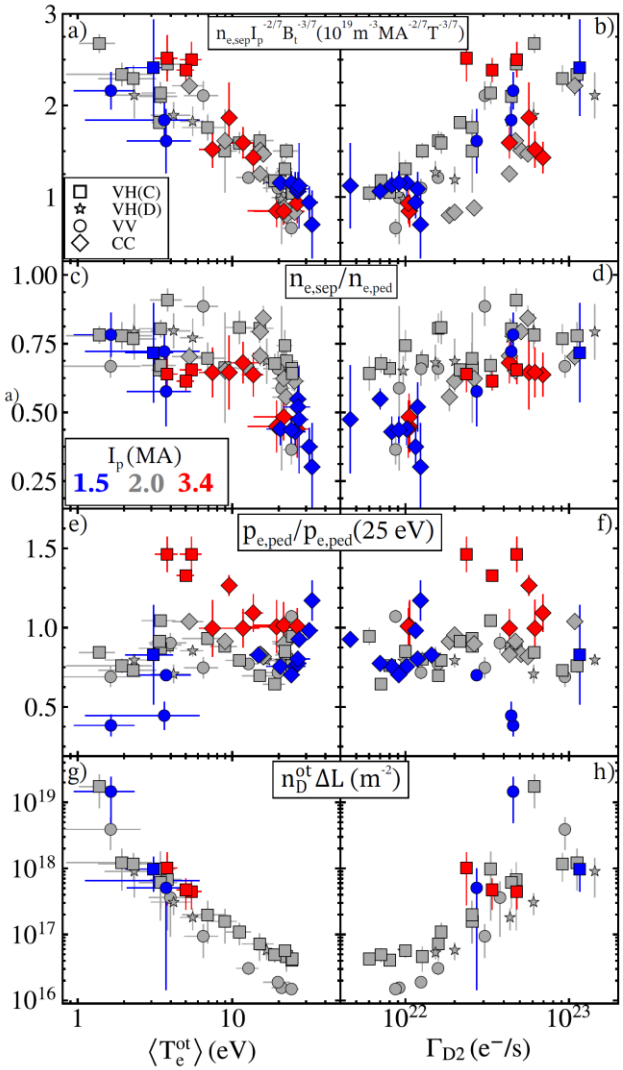

Figure 7: Correlations between $\langle T_{e,ot} \rangle$ (a,c,e,g) and D_2 gas fueling rate (b,d,f,h) and normalized separatrix density $n_{e,sep} I_p^{-2/7} B_t^{-3/7}$, ratio of the separatrix to pedestal densities, , pedestal pressure normalized by the pedestal pressure at $\langle T_{e,ot} \rangle$ =25 eV, and the product of atomic neutral density and effective Dα emission path length.

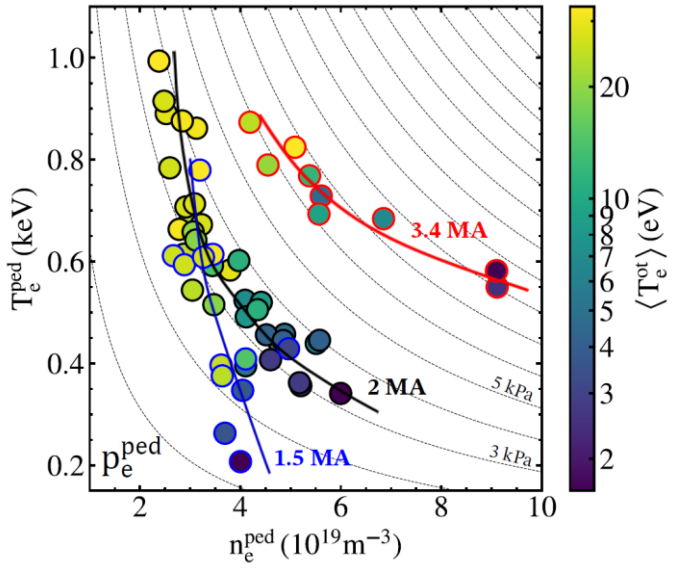

Figure 8: T_e^{ped} vs. n_e^{ped} for the three plasma current branches of the H-mode unseeded dataset. Data is plotted over constant p_e^{ped} isobar lines. Marker fill colors indicate the corresponding value of $\langle T_{e,ot} \rangle$ shown in the color bar.